PCCP

Accepted Manuscript

ROYAL SOCIETY OF CHEMISTRY

www.rsc.org/pccp

Physical Chemistry Chemical Physics RSCPublishing

ARTICLE

Characterization of Molybdenum Monomeric Oxide Species Supported on Hydroxylated Silica; A DFT Study

Cite this: DOI: 10.1039/x0xx00000x

Received ooth January 2012,
Accepted ooth January 2012

DOI: 10.1039/x0xx00000x

www.rsc.org/

Hazar Guesmi [a], Robert Gryboś[b], Jarosław Handzlik[c], Frederik Tielens[d,*]

Periodic DFT calculations have been performed on molybdenum(VI) oxide species supported on hydroxylated amorphous silica surface. The Mo grafting site has been investigated systematically on the type of silanol (geminate, vicinal, isolated or in a nest) accessible on the surface, as well as its effect on H-bond formation and stabilization, with the Mo-oxide species. Different grafting geometries, combined with different degrees of hydration of the Mo species are investigated using atomistic thermodynamics. The most stable Mo(VI) oxide species resulting from these calculations are confronted with experiment. Finally, calculated vibrational frequencies confirm the experimental evidence of the dominant presence of di grafted di-oxo Mo(VI) species on silica up to 700 K.

Introduction

Supported oxide catalysts are designed to maximize the number of active sites by reaching the dispersion limit of the two-dimensional support[1]. Typical supports are silica-, alumina-, titania- based materials, and molecular sieves. The physico-chemical properties and its low price make amorphous silica an ideal candidate for catalyst support. Many transition metal oxides have been deposited/grafted on various silica surfaces[2-5]. The structural characterization at the molecular level of an isolated transition metal species dispersed on the oxide support is of the utmost importance to unravel the catalytic reaction mechanism and in designing new high performing catalysts. In this study we focus on Mo(VI) monomers supported on silica.

Molybdenum species grafted on silica have attracted considerable attention because of their relevance to a variety of catalytic reactions, including the selective oxidations of alkanes[6, 7] alkenes[8], and alcohols[9, 10]. Many research groups have reported methods of characterization and synthesis which is supposed to generate specific surface molybdenum oxide species. At low coverage, the active sites have been proposed to have various structures, including isolated dioxo surface species[10-14] isolated mono-oxo species[15-18], and dimeric surface species[19] (See Fig. 1).

Characterization of Mo-oxide/silica catalyst has been the subject of considerable research[12, 15, 20-29], but very few studies are combined with a computational approach. Theoretically studies have been focused almost exclusively on mono-oxo and di-oxo species without OH groups mainly using cluster models and without considering a realistic amorphous silica model[30-34]. Mo-silica species have been calculated in detail by Chempath[28] and Handzlik[34, 35], from which it was concluded that mono-oxo species can be more stable under dehydrated conditions than the di-oxo species.

The objective of this study is to investigate possible atomic models of the silica supported Mo oxide catalysts in hydrated and dehydrated forms, in a similar way to our study on the characterization of vanadium[36] and chromium[37, 38] containing silica. To this end, density functional theory (DFT) is used to calculate the structures, vibrational frequencies, and relative stabilities of isolated monomeric Mo oxide species grafted to the surface of amorphous silica.

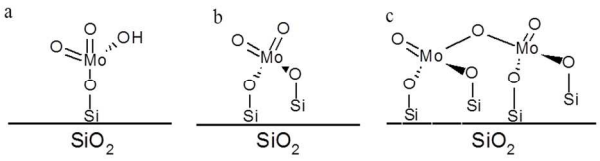

Figure 1. Schematic representation of a. Mono-oxo (mono-grafted) Mo oxide monomeric species b. Di-oxo (di-grafted) Mo monomeric species and c. tetra-oxo (tetra-grafted) dimeric species, all grafted on amorphous silica.

Methodology

Computational details

All calculations are performed using ab initio plane-wave pseudopotential approach as implemented in VASP[39, 40]. The Perdew-Burke-Ernzerhof (PBE) functional[41, 42] has been chosen to perform the periodic DFT calculations with an accuracy on the overall convergence tested elsewhere[43-46]. The valence electrons are treated explicitly and their interactions with the ionic cores are described by the Projector Augmented-Wave

method (PAW)[47, 48], which allows to use a low energy cut off equal to 400 eV for the plane-wave basis. The Gamma point is used in the Brillouin-zone integration. The positions of all the atoms in the super cell are relaxed until the total energy differences decrease below 10^{-4} eV (forces acting on atoms fall below 0.01 eV/Å).
Vibrational spectra have been calculated for selected surface species within the harmonic approximation. Only the molybdenum/tungsten centre and its first and second neighbours (O-Si and OH groups) are considered in the Hessian matrix. This matrix is computed by the finite difference method followed by a diagonalisation procedure. The eigenvalues of the resulting matrix lead to the frequency values. The assignment of the vibrational modes is done by inspection of the corresponding eigenvectors and a scaling factor was used according to Halls et al.[49]

2. Model description
The hydrated SiO2 containing 13 water molecules per unit cell was used, as in the original paper[50] and in our vanadium oxide/SiO_2[36], chromium oxide/SiO_2[37, 38] and gold/SiO_2[51, 52] studies. The silica model reproduces the experimentally established ring size distribution, Si-O-Si and O-Si-O angles, overall density of silanol groups and partition into several types (isolated, associated, geminate) (Fig. 2). Unit cell dimensions of model are 12.77 × 17.64 × 25.17 $Å^3$.
The group VI precursor is modelled by a H_2MoO_4 molecule (a model precursor). One such species is added to the silica unit cell resulting in a coverage of 0.44 monomers per nm2, a typical coverage found in working catalysts.[53]

In order to probe and compare various grafting sites on the silica surface, a di-oxo molybdenum monomer was used, in analogy to chromium, for which the di-oxo monomer was found to be most stable at 0 K [37, 38].
Next, a thermodynamic analysis was performed to establish what the most stable monomer form at different temperatures is. The model precursor H_2MO_4 is grafted by dehydration of surface silanols, following the reaction:

$$H_2MoO_4 + SiO_2(H_2Osurf)_{13} \rightarrow O_xMo(OH)_y\text{-}SiO_2(H_2Osurf)_{13-n} + n\,H_2O \quad (1)$$

The n = the number of water molecules added or eliminated and varies between -1 and +3, x = number of Mo=O groups and, y = number of Mo-OH groups, with the condition x + y = n + 3, due to the oxidation state of molybdenum. Theoretically up to four silanols may be involved in the reaction yielding different modes of grafting: mono, di, tri and tetra.
Structures involving different silanol types: isolated (Si-OH), vicinal (HO-Si-O-Si-OH), geminate (HO-Si-OH) and non-vicinal (two Si-OH groups not directly connected) on the surface were considered. Due to the flexibility of the silica surface, these species can be more or less easily accommodated.

Figure 2. A. Top view of the 2 × 2 unit cell (12.77 × 17.64 × 25.17 $Å^3$) of the amorphous silica van der Waals surface model, B. Di-oxo digrafted Mo(VI) oxide species grafted on silica. (Mo in green)

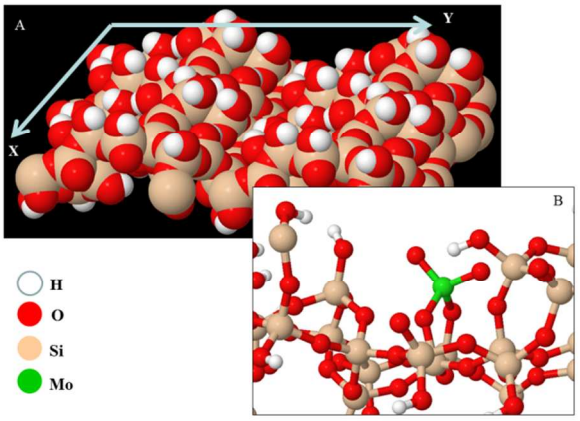

Results and Discussion

Survey of the grafting sites
On each site, the model precursor (H_2MoO_4) reacts with two silanol groups and creates two linkages with the surface, liberating two water molecules in the process. Possible anchoring sites are divided into three categories: (i) geminate – both silanol groups are located on the same Si centre, (ii) – vicinal – silanol groups are attached to silicon sites directly connected by an oxygen bridge and (iii) – non-vicinal – all other sites, in which silicon centres bearing silanol groups are spaced further apart. It is clear that non-vicinal sites are most flexible, while geminate sites are rather rigid. Almost all grafting energies are positive, reflecting the fact that, thermodynamically, monomers are unstable in the presence of water. On the other hand, in the process of slow, overnight drying at elevated temperature as is employed in the catalyst synthesis; monomers should occupy various grafting sites in the order given by the adsorption energies. It should be noted that precursors other than $MoO_2(OH)_2$ are usually used during catalyst preparation and that the monomer sites connected with the support are rather generated during the further calcination step; or organometallic precursors can also be used what can alter the thermodynamics of the grafting process. Therefore, the grafting reactions presented in this work should be considered as a way to compare energetic stability of the sites rather than the description of a real grafting process.

Usually, the Mo centre is bonded with four oxygen atoms in a slightly distorted tetrahedral symmetry. However, in few cases, nearby surface OH groups create Mo-OH-Si bridges and change the Mo coordination number to 5. If the structure is flexible enough, the monomer can attain a penta coordinated trigonal bi-pyramidal symmetry. Such structures will be discussed after the more common tetrahedron case.
In Table 1 we present the grafting energy for all geometries considered. Positive values indicate thermodynamically unstable adsorption. However, the monomer stays at the surface, due to a kinetic barrier. When two water molecules are available, monomers can detach from the surface as $MoO_2(OH)_2$ and create two silanol groups. When only one H_2O is present, the monomer leaves as MoO_3. If one allows for the possibility of creating Si-O-Si siloxane bridges, then two more situations can be envisioned: (i) with one water present the monomer leaves as $MoO_2(OH)_2$, (ii) with no water, the monomer leaves as MoO_3.

Figure 3. Amorphous silica surface modeled by two sides of the slab. The actual unit cell is shown as red rectangle. Pairs of silanol groups which are used to anchor a particular Mo monomer are connected with black lines (g – geminal, v – vicinal, n – non-vicinal).

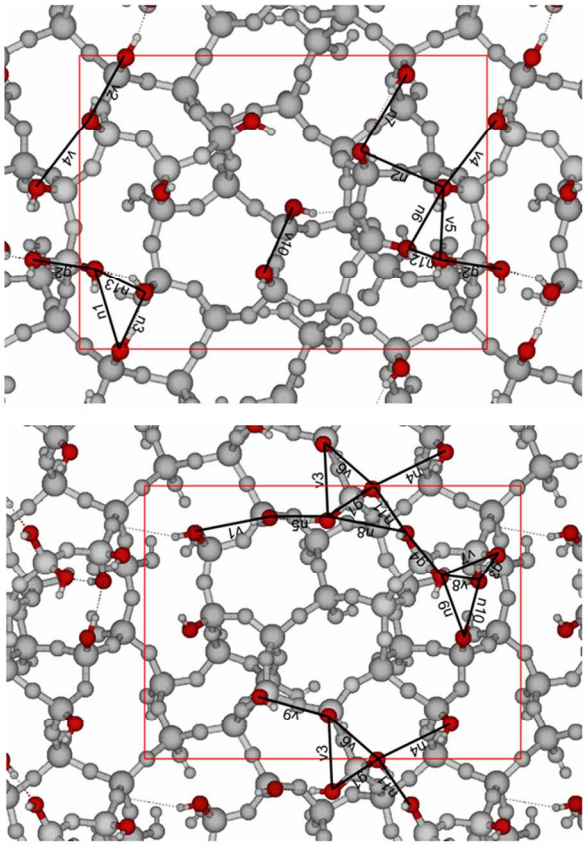

Table 1. Grafting energies of a di-oxo molybdenum monomer (structure F) on various sites on the surface of amorphous silica. Energies are calculated with respect to MoO_3 or $MoO_2(OH)_2$ in the gas phase. Negative values (in eV) indicate stable species.

Site label	MoO_3	$MoO_2(OH)_2$
Geminate sites		
g1	-1.16	1.73
g2	-1.46	1.44
g3	-1.59	1.30
g4	-1.36	1.53
Vicinal sites		
v1	-2.33	0.56
v2	-2.50	0.39
v3	-2.23	0.66
v4	-2.90	0.00
v5	-2.58	0.32
v6	-2.32	0.57
v7	-2.75	0.14
v8	-1.96	0.93
v9	-2.64	0.25
v10	-2.58	0.31
Non-vicinal sites		
n1	-3.06	-0.16
n2	-2.94	-0.05
n3	-2.96	-0.07
n4	-2.92	-0.02
n5	-2.78	0.11
n6	-2.53	0.36
n7	-2.86	0.03
n8	-2.44	0.45
n9	-2.73	0.16
n10	-2.97	-0.08
n11	-2.80	0.09
n12	-2.75	0.14
n13	-3.05	-0.16

For anchoring, geminate sites are energetically disfavoured due to their high rigidity. The adsorption energy is between 1.30 and 1.73 eV indicating an unstable structure. Vicinal sites are more flexible and can accommodate a Mo monomer with adsorption energies between 0.0 and 0.93 eV. Monomers are more stable on the flexible non-vicinal sites – all adsorption energies are below 0.36 eV. Few structures even show stable adsorption, although only barely stable as the best adsorption energy is only -0.16 eV. It seems that structures with more hydrogen bonds are more stable, but no clear correlation could be found. As noted above, without large excess of water vapour available, anchored monomers can only detach from the grafting sites as MoO_3 species. This reaction still requires one water molecule to recreate two surface hydroxyl groups. The monomer stability with respect to gaseous MoO_3 in the presence of traces of water is very high – energies required to remove a monomer from the surface range from 1.16 to over 3 eV. Without water, MoO_3 can still be removed if the anchoring Si centres are close enough to create a siloxane bridge. However, this reaction pathway is expected to require even more energy. It is interesting to note, that depending on the grafting site, the adsorption energy can vary by as much as 0.6 eV, or even 1.1 eV if one includes geminate sites.

The geometry of the monomer does not vary much between different grafting sites. The molybdenyl Mo=O bonds have lengths between 1.71 and 1.75 Å, depending on the number of hydrogen bonds between surface and the monomer. If no such hydrogen bonds are present, both Mo=O bonds are 1.72 Å. If two hydrogen bonds are created to one molybdenyl oxygen atom, then the corresponding Mo=O bond is weakened and elongated to 1.75 Å while the other Mo=O is contracted to 1.71 Å. The angle between Mo=O bonds is usually 107 – 108° with some deviations induced by hydrogen bonds (See Table 2).

The lengths of Mo-O(Si) bonds anchoring the monomer to the surface range from 1.87 to 1.95 Å. The angle between those bonds vary between 88° and 115° (for the very strained geminate sites it is 80° or less) and correlate well with the adsorption energy – monomers with angles close to the tetrahedral angle of 109° are usually more stable.

Table 2. Calculated geometrical parameters in Mo oxide/silica system. Distances in Å and angles in degrees.

Model	d(MoO-H)	d(Mo-Osi)	d(Mo=O)	O=Mo=O)
A	1.913	1.922		
	1.928			
	1.932			
	1.941			
	1.997			
B	1.902	1.951	1.739	
	1.914			
	1.921			
C	1.911	1.887	1.720	108.25
			1.728	
D	1.887	1.936		
	1.899	1.946		
	1.968			
	1.976			
E	1.916	1.910	1.712	
	1.948	1.932		
F	-	1.895	1.725	107.84
		1.892	1.725	
G	1.847	1.939		
	1.940	1.940		
	1.950	2.040		
H	1.918	1.896	1.722	
		1.905		
		1.955		
I	-	1.917	1.702	
		1.934		
		1.958		
		1.976		

As mentioned above, in few cases the coordination of Mo central atom is 5 instead of 4. A flexible OH group in the vicinity can create a Mo-OH-Si bridge and stabilize the monomer. However, at geminate and vicinal anchoring sites, the monomer itself is not flexible enough to fully adopt the desired trigonal bi-pyramid coordination and the imposed strain cancels out the effect of crating another oxygen bridge to the surface. Only on a non-vicinal site the Mo monomer exhibits distorted trigonal bi-pyramid geometry, with one axial bond elongated (the one to the surface OH group). In fact this structure was found to be the most stable. However, due to special surface arrangement necessary to accommodate such structure it will, most probably, not be the most common.

Mo-species at different temperatures

Figure 4 shows mono- (structure: A, B, C), di- (structure: D, E, F), tri- (structure: G, H) and tetra-grafted (structure: I) Mo-oxide species on silica support. Tri- and tetra-grafted species need the presence of three and four neighbouring silanol sites, respectively. The preference of mono-grafted species to the vicinal HO-Si-O-Si-OH, depend on the neighbourhood of the Mo-site, and is dependent on the possibility to form H-bonds between the metal oxide Mo-OH groups and surface silanol groups, which stabilize the conformations. Di-grafted metal oxide species show a large preference for vicinal silanol sites compared to non-vicinal and geminate ones (vide ultra).

According to the calculated energy values for reaction at 0 K (eq. 1) shown in Table 1, the tri- (species G and H) and tetra-grafted (species I) oxide species are the least thermodynamically stable configurations. The most stable structure is predicted to be the di-oxo mono-grafted species (species C): In our recent DFT study of the stability of grafted chromium species on silica support[37], the di-oxo mono-grafted Cr(VI) (structure analogous to F) was also predicted to be the most stable species.

Figure 4. Different geometries as a function of its hydration state for the supported Mo oxide grafted on amorphous silica.

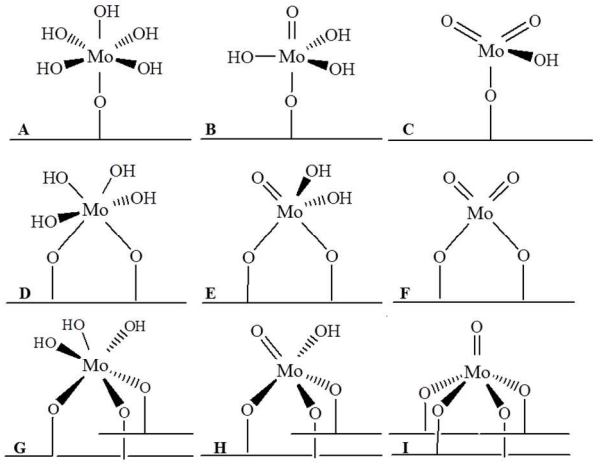

The geometrically optimized structures show Mo=O distances from 1.702 to 1.739 Å on the amorphous surface and between 1.713 to 1.750 Å on the crystalline triclinic silica(ref!!). Depending on the number of OH groups on the Mo atom (see Table 2). The lower the number of OH groups the shorter is the Mo=O bond. These calculated Mo=O values are larger than the experimental Mo=O bond distances reported for gas phase Mo compounds MoO_2Cl_2 (1.686 Å)[54] and $MoOCl_4$ (1.658 Å)[55].

The configuration of di-grafted and tetra-grafted molybdenum F and I (see Figure 4) represent the typical species reported in the literature for Mo(VI) in di-oxo and mono-oxo forms. Using EXAFS method for the characterization of molybdenum formed on silica Takenaka et al.[12] have suggested the existence of octahedral molybdenum species with four measured Mo-O bonds. The length of two shorter bonds was estimated to be 1.68 Å and that of the other bonds to be 1.88 Å. It is likely that the shorter Mo-O bonds have a double bond character and would be terminal ones, and the longer bonds would be bound directly to the silica support. Concerning the penta-coordinated mono-oxo species, its presence was a subject of controversies. While some theoretical works[28, 34] predicted the mono-oxo species to be energetically favourable under dehydrated conditions, from experimental point of view its presence was

proposed based on the failure to observe more than two bands in the Raman spectrum of isolated molybdate species that had been partially exchanged with $O18$[26, 56]. Nevertheless, the reason these bands were not observed was explained by Chempath et al.[30, 31], later, they were observed by Lee et al.[3] who proposed that di-oxo Mo species are dominant on silica. The mono-grafted Mo configuration (species C) can be formally regarded as the product of successive hydration of configuration I and F. Its stability might mainly results from hydrogen interaction with silanol groups.

Energetics of the supported Mo oxide species

Grafting of Mo metal oxide species on silica surface has a relatively small effect on the silica framework, and is comparable with what has been found in our previous study on the grafting of vanadium and chromium oxide species on silica.[36-38]

Depending on their density, surface silanols are generally interacting with their neighbours forming an H-bond network. The grafting reaction perturbs the local H-bond network in two ways: first, surface hydroxyl groups are removed upon grafting and secondly, the Mo oxide units might also form hydrogen bonds with the silica support. In the models studied, the M-OH groups bind to surface silanols with a stabilization of the structure, in contrast to M=O groups which are found to be H-bond free on the amorphous surface.

To summarize, the nature of the silanol group (isolated, vicinal, and geminate) has indeed an influence on the geometry and stability of the grafted precursor. The type of silanol becomes critical for the mono-grafted species, since they are the only species that can bind on every silanol group, independently of its type and its number of local neighbours. However, statistically an area of the silica surface with a high number of silanols will accommodate more precursors. The only restriction on grafting is the availability of silanol groups on the surface. So, if local silanol nests are present it will be the anchoring site with the highest probability, just based on numbers and not on energies.

The overall silica framework is only slightly modified upon metal oxide grafting. The tri- and tetra grafted sites introduce the largest strain on the silica surface. However, the silanol H-bond connectivity influences the overall reaction energy. The final result depends on the energetic balance of the number of H-bonds broken/created.

Considering the reaction energy ΔE_{react} of Table 3 calculated according to the eq. 1 for the best grafting modes as a function of hydration rate. For Mo oxide the values of -0.49, -0.26, -0.76, +0.02, and +0.38 eV, for +1, 0, -1, -2 and -3 water molecules are obtained, corresponding to the models A, B, C, F, and I, respectively. As from -2 water molecules the grafting energies are positive, indicating that the adsorption of the H_2MO_4 is disfavoured compared to the initial situation (hydroxylated silica and H_2MO_4 in the gas phase).

Table 3. Reaction energy calculated using equation (1) for the grafting of the different group VI metal oxide models investigated. (Values in eV).

Model	ΔE_{react}	ΔE_{react}[38]
Group VI metal	Mo	Cr
A: Surface + MO_4H_2 + $1H_2O$	-0.49	-0.26
B: Surface + MO_4H_2	-0.26	-0.89
C: Surface + MO_4H_2 - $1H_2O$	-0.76	-2.09
D: Surface + MO_4H_2	-0.18	0.13
E: Surface + MO_4H_2 + $1H_2O$	-0.39	-0.80
F: Surface + MO_4H_2 – $2H_2O$	0.02	-1.33
G: Surface + MO_4H_2 - $1H_2O$	1.04	1.72
H: Surface + MO_4H_2 –2 H_2O	1.06	0.34
I: Surface + MO_4H_2 – 3 H_2O	0.38	0.42

Another point which is revealed by this reaction energy analysis, is that the most favourable models associated to the different degrees of hydration are different between Cr and Mo. Nevertheless, it should be noted that the results in Table 3 report electronic energies only, which are identical to the free energy at 0 K. Under given temperature T and pressure p, the contributions of entropy and chemical potentials have to be taken into account in the free energies.

It is interesting to note that the synthesis of the grafted M(VI)-SiO_2 catalyst occurs experimentally through successive steps: after impregnation by the precursor at room temperature, in aqueous or non-aqueous solution, the obtained surface is dried and then calcined to achieve a chemically grafted active site and to burn all reactive species still present at the surface. In the cases of the M(VI)-SiO2 synthesis, the samples are dried one night at room temperature or at 383 K, then calcined for several hours up to 923 K[37, 57] depending on the experimental works[3, 57-59] and references therein. Thus, it is empirically known that a high temperature and dehydration conditions are necessary to obtain the multi-grafted group VI transition metal-complexes.

In order to get a more precise picture of the respective stabilities of the mono-, di-, tri and tetra-grafted Mo(VI) species on the silica surface, we performed calculations using the atomistic thermodynamics approach. To take into account deviations in surface composition and the presence of gas phase, one introduces appropriate chemical potentials to calculate an approximation of the Gibbs free-surface energy. Assuming that the surface is in thermodynamic equilibrium with the gas phases, the chemical potentials are related to a given temperature T and pressure p. This procedure enables to extend the 0 K and zero pressure DFT results to experimentally relevant environments, thereby bridging the gap between ultra-high vacuum like conditions, and temperatures and gas phase pressures that are applied in realistic catalytic conditions.

The Mo(VI)/silica system is considered in contact with a gaseous water reservoir. From the electronic energy, the free energy of the water/Mo(VI)/silica interface under known thermodynamic conditions may be estimated following the approximations used by Digne et al.[60], as originating from Kaxiras et al.[61] and Qian et al.[62]. It consists in the neglect of the variation of the chemical potentials of the surfaces with the adsorption and the consideration of the gas phase as a perfect gas. In the proposed scheme, the free energy of water (including the ZPE correction) in the gas phase is:

$$\Delta G(H_2O) = E(H_2O) - ((\Delta H_G - T\Delta S_G(T)) + RT \ln (p/p°)) \quad (2)$$

where $E(H_2O)$ is the electronic energy of water calculated at 0 K, ΔH_G and $\Delta S_G(T)$ are the enthalpy and entropy of gaseous water, calculated with the Gaussian03 code[63] as a function of the temperature, p is the partial pressure of water vapour and p° is the standard pressure (1 bar).

Using the above mentioned formalism, the free energy of dehydration reaction (eq. 1) for the formation of the mono-, di-, tri and tetra-grafted Mo(VI) complexes at equilibrium conditions, are then expressed as:

$\Delta G1 = E(\text{model A}) - 1.\Delta G(H_2O) - E((\text{Si-O})\text{Slab}) - E(O_2M(OH)_2)$ (3)

$\Delta G2 = E(\text{model B or D}) - E((\text{Si-O})\text{Slab}) - E(O_2M(OH)_2)$ (4)

$\Delta G3 = E(\text{model C, E, G}) + 1.\Delta G(H_2O) - E((\text{Si-O})\text{Slab}) - E(O2M(OH)2)$ (5)

$\Delta G4 = E(\text{model F or H}) + 2.\Delta G(H_2O) - E((\text{Si-O})\text{Slab}) - E(O_2M(OH)_2)$ (6)

$\Delta G5 = E(\text{model I}) + 3.\Delta G(H_2O) - E((\text{Si-O})\text{Slab}) - E(O_2M(OH)_2)$ (7)

In this approach, we consider that the energies of the different types of grafting transitions are independent of the degree of hydration of the silica surface. It is known experimentally that silanols are stable at silica surfaces until 673 K. Above this temperature, silanols begin to condensate into siloxane bridges[64]. Thus, our model with 5.8 OH/nm^2 corresponding to conditions of a hydroxylated surface, remains valid until the temperature of 673 K.

Figures 5 shows the surface free energy Γ, defined as the free energy per surface area, of the mono-, di-, tri- and tetra-grafted Mo(VI)-complexes on the silica surface as a function of temperature (T) for a water partial pressure (p) equivalent to the ambient air water partial pressure (pw = 1500 Pa)[65].
At these conditions, for Mo the mono-grafted model C containing two Mo=O groups and one Mo-OH group is predicted to be the dominating specie at low temperatures (up to 80 K). For T > 80 K the tetra-grafted Mo=O model I (See dotted line Fig. 5) is omnipresent, until the validity of our model is reached due to dehydration the surface. Our model is predicted to applicable only up to 673 K. (Figure 5),
Nevertheless, tetra grafted species I can also be considered as a model for the insertion/substitution of Mo into silica, which is not reached in the synthesis of the usual Mo-oxide/silica catalysts. This tetra grafted species can be formed if four silanol groups are available in such a configuration (into a nest) that the Mo precursor can react with the surface. In other words model I is only possible in special situations in which the silanol local density it permits.

Figure 5. Phase diagram (surface energy vs. temperature) showing the stability ranges for the different grafted Mo oxide geometries.

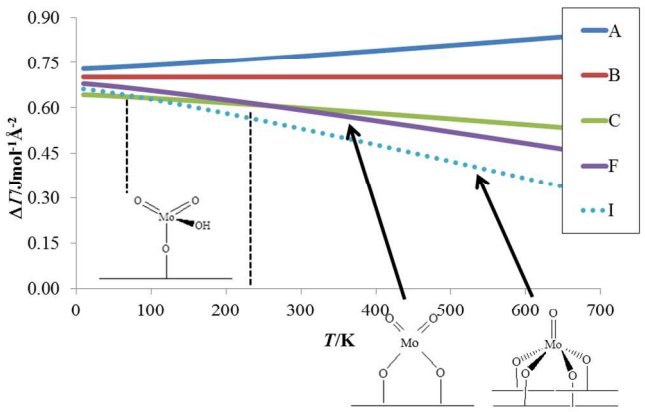

Taking this into account the most stable species is then the di-grafted di-oxo species F model (See Fig. 4), for temperatures higher than 290 K. These result is fully consistent with the experimental procedure used in the synthesis of Mo(VI)-supported catalysts by the grafting method[3], where samples are heated and annealed at high temperatures to obtain O=Mo=O surface structures. Note that such species correspond to completely dehydrated conditions. In hydrated conditions (high water pressure or low temperature) mono-grafted model with an extra Mo-OH group is stabilized.
In summary, the mainly two grafted Mo(VI) species may exist on a silica surface depending on the experimental conditions. They are supposed to reversibly interconvert in the presence of water, and they might coexist on the surface.

Vibrational frequency analysis

Lee and Wachs[2, 3] concluded that under dehydrated conditions the Mo(VI) oxide forms on silica are predominantly present as isolated dioxo species, whereas the isolated monooxo Mo(VI) species are in minority on the surface. Nevertheless, Molybdenum species might be present as mono – di-, oligomeric oxide species and monocrystalite. Experimentally this point is still under debat.[66]
Comparing the theoretical frequencies with the experimental ones[2, 3], we can conclude that the model containing the most similarities with the experiment is model F. This was concluded with the use of a scaling factor for the frequencies, independently from the type of bond and normalized on the well-known silanol vibration. This approach has been used with success in former studies.[67-69]
According to Lee et al.[2, 3] the surface molybdenum oxide species on the supported MoO_3/SiO_2 catalyst are present as both dioxo $(O=)_2Mo(\text{-O-Si})_2$ and monoxo $O=Mo(\text{-O-Si})_4$ surface species, giving rise to Raman bands for ν_{sym} (Mo(=O)2) at 976 - 988 cm^{-1} and ν_{sym} (Mo=O) at 1020 cm^{-1}.[6, 16, 19, 24] The corresponding asymmetric ν_{asym} (Mo(=O)$_2$) vibration appears as a shoulder at 965 - 975 cm^{-1} and the bending δ(O-Mo-O) mode at 364 cm^{-1}.[22, 24]
The calculated vibrational frequencies are tabulated in Table 4. Vibrational analysis shows that the Mo=O bond vibrations are not as cleanly decoupled from others as was in the case of chromium[37]. Only the frequency of Mo=O asymmetric vibration can be easily given. It ranges from 973 to 1001 cm^{-1} due to various hydrogen bonds arrangements, which in turn depend on the hydration level. In effect, a wide band cantered

around 991 cm^{-1} should appear in the spectrum. From these results one can conclude that the vibrational frequencies calculated for model structure F confirm the experimental results presented in refs.[2, 3]

Table 4. Scaled (0.96) and unscaled calculated vibrational frequencies for M=O group.in mono or di oxo-configuration in the different models studied. (Frequencies in cm^{-1}).

	Mo=O	Mo=O (scaled)	Exp.[3]
B	997	957	
C(ν_{sym})	1038	997	
C(ν_{asym})	1005	965	
E	1048	1006	
F(ν_{sym})	1028	987	976 - 988
F(ν_{asym})	1015	975	965 - 976
H	1020	979	
I	1066	1024	1020

Conclusions

A DFT atomistic thermodynamics approach combined with experimental and theoretical vibration frequency analysis enabled us to describe Mo(VI)-oxide/silica system. This step forward enabled to shed some light on a question open for some decades now: Which Mo(VI) oxide species is the most common on an amorphous silica surface? From our calculations we predicted that di-oxo digrafted Mo-oxide species are expected to be the dominant species in dehydrated conditions over a large range of temperatures (T > 290 K). At lower temperatures (T < 290 K) a monografted di-oxo Mo oxide species appears. If during the grafting high density silanol domains are present, showing nests of at least four silanol groups, a mono-oxo tetra grafted species might also be formed. Although, the latter species is thermodynamically stable, its presence is merely due to the distribution of the silanol density on the silica surface.

A good agreement between calculated and experimental vibrational frequencies was found for the di-oxo di-grafted Mo-species.

Another aim of this study has been reached since it was the construction of a realistic and calculable (periodic DFT level) structure representing Mo(VI) oxides supported on amorphous silica. With this model the investigation of its reactivity (transition states and reaction paths) will be possible for a series of important reactions, as mentioned in the introduction.

Acknowledgements

This work was performed using HPC resources from GENCI-[CCRT/CINES/IDRIS] (Grant 2014-[x2014082022]) and the CCRE of Université Pierre et Marie Curie. Dr. B. Diawara from LCPS ENS Paris is kindly acknowledged for providing us with ModelView used in the visualization of the structures. RG acknowledges support from Polish National Science Centre under grant no. 2011/03/B/ST4/.

Notes and references

[a] CNRS-UM2-ENSCM-UM1, UMR 5253, Institut Charles Gerhardt Montpellier, Ecole Nationale Supérieure de Chimie de Montpellier, 8 rue de l'Ecole Normale, 34296 Montpellier, France

[b] J. Haber Institute of Catalysis and Surface Chemistry, Niezopominajek 8, 30-239 Kraków, Poland

[c] Faculty of Chemical Engineering and Technology, Cracow University of Technology,
ul. Warszawska 24, 31-155 Kraków, Poland

[d] Sorbonne Université, UPMC Univ Paris 06, UMR 7574, Laboratoire Chimie de la Matière Condensée, Collège de France, 11 place Marcelin Berthelot, 75231 Paris Cedex 05, France

*Corresponding author: F. Tielens, e-mail: frederik.tielens@upmc.fr

1. I. E. Wachs, *Catalysis Today*, 1996, **27**, 437-455.
2. E. L. Lee and I. E. Wachs, *Journal of Physical Chemistry C*, 2007, **111**, 14410-14425.
3. E. L. Lee and I. E. Wachs, *Journal of Physical Chemistry C*, 2008, **112**, 6487-6498.
4. P. Michorczyk and J. Ogonowski, *Chemical Communications*, 2012, **48**, 7283-7285.
5. P. Michorczyk, P. Pietrzyk and J. Ogonowski, *Microporous and Mesoporous Materials*, 2012, **161**, 56-66.
6. N. D. Spencer, C. J. Pereira and R. K. Grasselli, *Journal of Catalysis*, 1990, **126**, 546-554.
7. M. A. Banares, J. L. G. Fierro and J. B. Moffat, *Journal of Catalysis*, 1993, **142**, 406-417.
8. N. Giordano, M. Meazza, A. Castellan, J. C. J. Bart and V. Ragaini, *Journal of Catalysis*, 1977, **50**, 342-352.
9. T. Ono, M. Anpo and Y. Kubokawa, *Journal of Physical Chemistry*, 1986, **90**, 4780-4784.
10. C. Louis, J. M. Tatibouet and M. Che, *Journal of Catalysis*, 1988, **109**, 354-366.
11. A. N. Desikan, L. Huang and S. T. Oyama, *Journal of the Chemical Society-Faraday Transactions*, 1992, **88**, 3357-3365.
12. S. Takenaka, T. Tanaka, T. Funabiki and S. Yoshida, *Journal of Physical Chemistry B*, 1998, **102**, 2960-2969.
13. D. S. Kim, M. Ostromecki and I. E. Wachs, *Catalysis Letters*, 1995, **33**, 209-215.
14. D. S. Kim, M. Ostromecki and I. E. Wachs, *Journal of Molecular Catalysis a-Chemical*, 1996, **106**, 93-102.
15. M. Deboer, A. J. Vandillen, D. C. Koningsberger, J. W. Geus, M. A. Vuurman and I. E. Wachs, *Catalysis Letters*, 1991, **11**, 227-239.
16. C. C. Williams, J. G. Ekerdt, J. M. Jehng, F. D. Hardcastle and I. E. Wachs, *Journal of Physical Chemistry*, 1991, **95**, 8791-8797.
17. C. Louis, M. Che and M. Anpo, *Journal of Catalysis*, 1993, **141**, 453-464.
18. M. A. Banares, H. C. Hu and I. E. Wachs, *Journal of Catalysis*, 1994, **150**, 407-420.
19. Y. Iwasawa, *Advances in Catalysis*, 1987, **35**, 187-264.
20. M. A. Banares and I. E. Wachs, *Journal of Raman Spectroscopy*, 2002, **33**, 359-380.
21. T. Ono, H. Kamisuki, H. Hisashi and H. Miyata, *Journal of Catalysis*, 1989, **116**, 303-307.
22. G. Mestl and T. K. K. Srinivasan, *Catalysis Reviews-Science and Engineering*, 1998, **40**, 451-570.
23. M. Anpo, M. Kondo, S. Coluccia, C. Louis and M. Che, *Journal of the American Chemical Society*, 1989, **111**, 8791-8799.

24. F. Arena and A. Parmaliana, *Accounts of Chemical Research*, 2003, **36**, 867-875.
25. M. Cornac, A. Janin and J. C. Lavalley, *Polyhedron*, 1986, **5**, 183-186.
26. H. C. Hu, I. E. Wachs and S. R. Bare, *Journal of Physical Chemistry*, 1995, **99**, 10897-10910.
27. Y. Iwasawa and S. Ogasawara, *Journal of the Chemical Society-Faraday Transactions I*, 1979, **75**, 1465-1476.
28. R. Radhakrishnan, C. Reed, S. T. Oyama, M. Seman, J. N. Kondo, K. Domen, Y. Ohminami and K. Asakura, *Journal of Physical Chemistry B*, 2001, **105**, 8519-8530.
29. B. N. Shelimov, A. N. Pershin and V. B. Kazansky, *Journal of Catalysis*, 1980, **64**, 426-436.
30. S. Chempath and A. T. Bell, *Journal of Catalysis*, 2007, **247**, 119-126.
31. S. Chempath, Y. H. Zhang and A. T. Bell, *Journal of Physical Chemistry C*, 2007, **111**, 1291-1298.
32. L. J. Gregoriades, J. Dobler and J. Sauer, *Journal of Physical Chemistry C*, 2010, **114**, 2967-2979.
33. C. S. Guo, K. Hermann, M. Havecker, J. P. Thielemann, P. Kube, L. J. Gregoriades, A. Trunschke, J. Sauer and R. Schlogl, *Journal of Physical Chemistry C*, 2011, **115**, 15449-15458.
34. J. Handzlik, *Chemical Physics Letters*, 2009, **469**, 140-144.
35. J. Handzlik and J. Ogonowski, *Journal of Physical Chemistry C*, 2012, **116**, 5571-5584.
36. M. M. Islam, D. Costa, M. Calatayud and F. Tielens, *Journal of Physical Chemistry C*, 2009, **113**, 10740-10746.
37. J. Handzlik, R. Grybos and F. Tielens, *Journal of Physical Chemistry C*, 2013, **117**, 8138-8149.
38. H. Guesmi and F. Tielens, *Journal of Physical Chemistry C*, 2012, **116**, 994-1001.
39. G. Kresse and J. Hafner, *Physical Review B*, 1993, **47**, 558-561.
40. G. Kresse and J. Hafner, *Physical Review B*, 1994, **49**, 14251-14269.
41. J. P. Perdew, K. Burke and M. Ernzerhof, *Physical Review Letters*, 1996, **77**, 3865-3868.
42. J. P. Perdew, K. Burke and M. Ernzerhof, *Physical Review Letters*, 1997, **78**, 1396-1396.
43. F. Tielens, M. Trejda, M. Ziolek and S. Dzwigaj, *Catalysis Today*, 2008, **139**, 221-226.
44. F. Tielens, M. Calatayud, S. Dzwigaj and M. Che, *Microporous and Mesoporous Materials*, 2009, **119**, 137-143.
45. N. Folliet, C. Roiland, S. Begu, A. Aubert, T. Mineva, A. Goursot, K. Selvaraj, L. Duma, F. Tielens, F. Mauri, G. Laurent, C. Bonhomme, C. Gervais, F. Babonneau and T. Azais, *Journal of the American Chemical Society*, 2011, **133**, 16815-16827.
46. F. Tielens, J. Andres, T. D. Chau, T. V. de Bocarme, N. Kruse and P. Geerlings, *Chemical Physics Letters*, 2006, **421**, 433-438.
47. P. E. Blochl, O. Jepsen and O. K. Andersen, *Physical Review B*, 1994, **49**, 16223-16233.
48. G. Kresse and D. Joubert, *Physical Review B*, 1999, **59**, 1758-1775.
49. M. D. Halls, J. Velkovski and H. B. Schlegel, *Theoretical Chemistry Accounts*, 2001, **105**, 413-421.
50. F. Tielens, C. Gervais, J. F. Lambert, F. Mauri and D. Costa, *Chemistry of Materials*, 2008, **20**, 3336-3344.
51. A. Wojtaszek, I. Sobczak, M. Ziolek and F. Tielens, *Journal of Physical Chemistry C*, 2010, **114**, 9002-9007.
52. A. Wojtaszek, I. Sobczak, M. Ziolek and F. Tielens, *Journal of Physical Chemistry C*, 2009, **113**, 13855-13859.
53. E. M. E. van Kimmenade, A. E. T. Kuiper, K. Tamminga, P. C. Thune and J. W. Niemantsverdriet, *Journal of Catalysis*, 2004, **223**, 134-141.
54. H. Thomassen and K. Hedberg, *Journal of Molecular Structure*, 1992, **273**, 197-206.
55. K. Iijima and S. Shibata, *Bulletin of the Chemical Society of Japan*, 1975, **48**, 666-668.
56. N. Ohler and A. T. Bell, *Journal of Physical Chemistry B*, 2005, **109**, 23419-23429.
57. E. Groppo, C. Lamberti, S. Bordiga, G. Spoto and A. Zecchina, *Chemical Reviews*, 2005, **105**, 115-183.
58. T. J. Dines and S. Inglis, *Physical Chemistry Chemical Physics*, 2003, **5**, 1320-1328.
59. W. K. Jozwiak, W. Ignaczak, D. Dominiak and T. P. Maniecki, *Applied Catalysis a-General*, 2004, **258**, 33-45.
60. M. Digne, P. Sautet, P. Raybaud, P. Euzen and H. Toulhoat, *Journal of Catalysis*, 2002, **211**, 1-5.
61. E. Kaxiras, Y. Baryam, J. D. Joannopoulos and K. C. Pandey, *Physical Review B*, 1987, **35**, 9625-9635.
62. G. X. Qian, R. M. Martin and D. J. Chadi, *Physical Review B*, 1988, **38**, 7649-7663.
63. M. J. Frisch, G. W. Trucks, H. B. Schlegel, G. E. Scuseria, M. A. Robb, J. R. Cheeseman, J. Montgomery, J. A., T. Vreven, K. N. Kudin, J. C. Burant, J. M. Millam, S. S. Iyengar, J. Tomasi, V. Barone, B. Mennucci, M. Cossi, G. Scalmani, N. Rega, G. A. Petersson, H. Nakatsuji, M. Hada, M. Ehara, K. Toyota, R. Fukuda, J. Hasegawa, M. Ishida, T. Nakajima, Y. Honda, O. Kitao, H. Nakai, M. Klene, X. Li, J. E. Knox, H. P. Hratchian, J. B. Cross, V. Bakken, C. Adamo, J. Jaramillo, R. Gomperts, R. E. Stratmann, O. Yazyev, A. J. Austin, R. Cammi, C. Pomelli, J. W. Ochterski, P. Y. Ayala, K. Morokuma, G. A. Voth, P. Salvador, J. J. Dannenberg, V. G. Zakrzewski, S. Dapprich, A. D. Daniels, M. C. Strain, O. Farkas, D. K. Malick, A. D. Rabuck, K. Raghavachari, J. B. Foresman, J. V. Ortiz, Q. Cui, A. G. Baboul, S. Clifford, J. Cioslowski, B. B. Stefanov, G. Liu, A. Liashenko, P. Piskorz, I. Komaromi, R. L. Martin, D. J. Fox, T. Keith, M. A. Al-Laham, C. Y. Peng, A. Nanayakkara, M. Challacombe, P. M. W. Gill, B. Johnson, W. Chen, M. W. Wong, C. Gonzalez and J. A. Pople, *Gaussian 03, Revision C.02*, Gaussian, Inc., Wallingford CT, 2004.
64. V. Bolis, B. Fubini, L. Marchese, G. Martra and D. Costa, *Journal of the Chemical Society-Faraday Transactions*, 1991, **87**, 497-505.
65. A. Guyot, G. E. Curtis and W. Libbey, *Smithsonian Meteorological Tables: Based on Guyot's Meteorological and Physical Tables*, 1896.
66. J. P. Thielemann, T. Ressler, A. Walter, G. Tzolova-Muller and C. Hess, *Applied Catalysis a-General*, 2011, **399**, 28-34.
67. F. Tielens, M. M. Islam, G. Skara, F. De Proft, T. Shishido and S. Dzwigaj, *Microporous and Mesoporous Materials*, 2012, **159**, 66-73.
68. F. Tielens, T. Shishido and S. Dzwigaj, *Journal of Physical Chemistry C*, 2010, **114**, 9923-9930.

69. F. Tielens, T. Shishido and S. Dzwigaj, *Journal of Physical Chemistry C*, 2010, **114**, 3140-3147.

Table of Contents Figure